Passive EM Processing of MEGATEM and HELITEM Data

Daniel Sattel *
EM Solutions LLC
Golden, CO 80401
dsattel@comcast.net

Eric Battig
BHP Billiton
Brisbane, QLD
eric.ee.battig@bhpbilliton.com

SUMMARY

The recording of raw or streamed data, as done by CGG during MEGATEM and HELITEM surveys, allows for the extraction of passive EM responses, inadvertently recorded during AEM surveys. These include powerline responses in data sets acquired in the vicinity of strong powerlines, VLF responses in data sets recorded with sufficiently high sampling frequencies and potentially AFMAG responses in the frequency range 25-600 Hz.

The recording of the three-component AEM data allows for the vector processing of these passive EM responses, including the derivation and modelling of the tipper data. Conductivity information can be derived from the tipper data with an apparent conductivity transformation and, more rigorously, with 2D and 3D inversions that take into account the terrain's topography.

The extraction of passive EM responses is demonstrated on a number of data sets. A powerline apparent-conductivity grid derived from a MEGATEM survey near Timmins, Canada indicates conductivity structures not evident in the corresponding active-source EM data. VLF responses derived from South American MEGATEM and North American HELITEM data show a strong correlation to topography. The former were successfully modelled with 2D and 3D inversions, and the derived shallow conductivity structures confirm and complement the information extracted from the active-source EM data.

Key words: AFMAG, airborne electromagnetics, data processing, inversion, VLF.

INTRODUCTION

The recording of streamed data allows for the thorough analysis of EM data (Lane *et al*., 1998), for the reprocessing of the active-source EM data (Sattel and Battig, 2016) and for the extraction and modelling of passive EM responses from powerlines, natural fields and radio fields ranging from audio-frequencies (AF) to very-low frequencies (VLF) and low frequencies (LF).
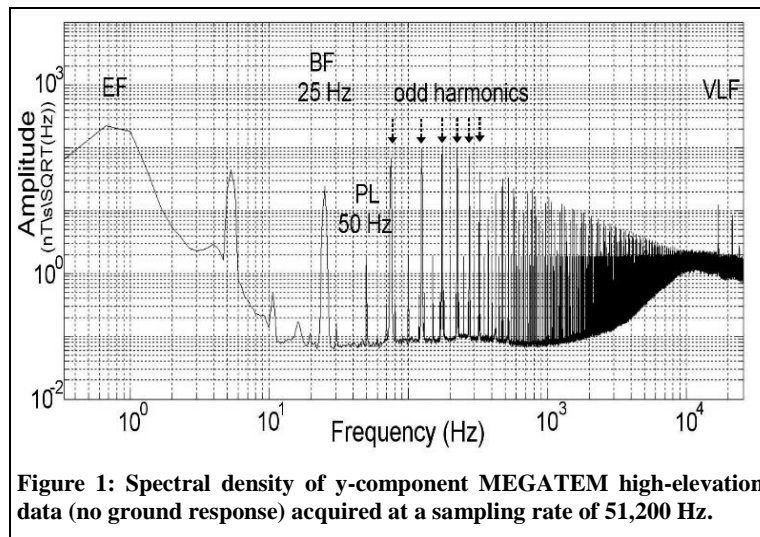
If there is enough coverage of powerline signal in a survey area, the corresponding ground EM response at 50 Hz and odd harmonics can be modelled and interpreted (Labson and Medberry, 1989). Vallee *et al*. (2010) discuss powerline apparent-conductivity grids, derived from raw MEGATEM data, which delineate structures not apparent on the standard MEGATEM EM amplitude and time-constant grids. The H-field emitted by powerlines may be horizontally polarized at distances of several miles from the powerline (Ward, 1966). In that case, tipper data can be derived from the x, y and z-component responses at 50 Hz and odd harmonics and be treated as AFMAG data.

Audio-frequency magnetics (AFMAG) is a geophysical method that analyses magnetic field data in the frequency range 1-1000 Hz, associated with the natural EM fields of lightning discharges. An airborne AFMAG system, such as ZTEM (Legault, 2012) measures responses in the frequency range 25-600 Hz or 30-720 Hz, depending on the frequency of the electric power grid. Natural-field EM responses above the spectral-density low at 1-2 kHz (Labson *et al*., 1985) might also contain useful information at frequencies in the VLF (3-30 kHz) and LF (30-300 kHz) ranges. The VLF method relies on EM signals transmitted by VLF stations operated by navies around the globe in the frequency range 15-30 kHz. The radiofrequency EM (RF-EM) method (Bosch and Műller, 2005) extends this range to frequencies in the LF range, which includes radio fields transmitted for navigation and communication purposes by naval and commercial radio stations. The recording of 3 components of the magnetic field data at AFMAG, VLF and LF frequencies allows for the derivation of tipper data and the application of 2D and 3D inversions (Holtham and Oldenburg, 2010; Sattel and Witherly, 2012; Kamm and Pedersen, 2014).

The digitisation rates of most active-source AEM systems are high enough to analyse VLF and even LF responses. One of the examined MEGATEM data sets provided to us by the GSC was recorded and stored at 184 kHz. The SkyTEM system uses a sampling rate of 5 MHz, but responses are gated in real time to reduce the data volume (Nyboe *et al*., 2017). Therefore, AFMAG, VLF and LF responses can potentially be extracted from streamed data recorded by active-source AEM systems. The main challenges are the variable receiver coil attitude and the extraction of these responses in the presence of the strong active-source EM signal.

We have examined powerline, AFMAG, VLF and LF responses for a number of AEM data sets, including MEGATEM data acquired in 2013 in South America by BHP Billiton and MEGATEM and HELITEM data acquired in various Canadian locations by the Geological Survey of Canada (GSC). The information gained from these passive EM responses is expected to complement the conductivity structure derived from the active-source EM data.

The power spectrum of the South-American MEGATEM data, recorded at high-elevation, is shown in Figure 1. It shows coil-motion or earth-field (EF) noise at frequencies below 25 Hz, the active-source signal at the base-frequency of 25 Hz (BF) and corresponding odd harmonics, the powerline noise at 50 Hz (PL) and odd harmonics (lower in amplitude than the active-source signal) and in the frequency-range from 16-25 kHz the VLF responses. Peaks at powerline and VLF frequencies indicate that there is potential for passive EM data processing for this data set.

Figure 1: Spectral density of y-component MEGATEM high-elevation data (no ground response) acquired at a sampling rate of 51,200 Hz.
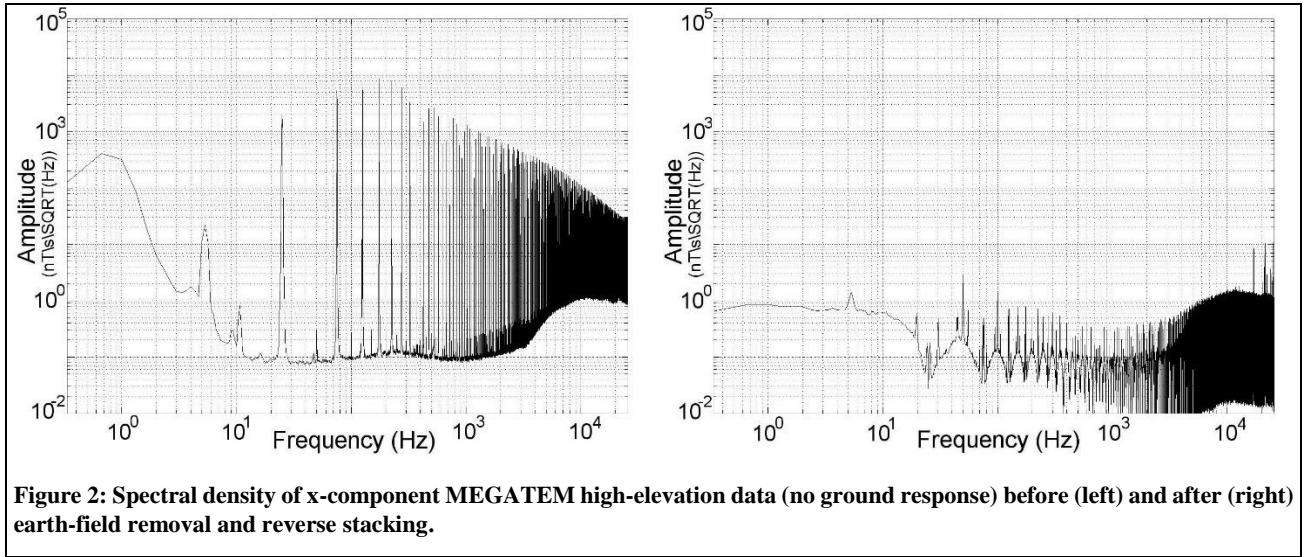
PASSIVE EM PROCESSING

Generally, the powerline and VLF signals recorded during active-source EM surveys are considered as noise, and attempts are made to reduce the impact on the EM signal. EM data contamination due to VLF noise is generally less obvious than powerline noise, but can be significant at the earliest time channels (Macnae, 2015; Rasmussen *et al*., 2017). The opposite approach is described herein, where the powerline, AFMAG and VLF signals are first extracted from the streamed active-source EM data and then modelled to derive conductivity structures of the surveyed areas.

Earth-field Removal and Reverse Stacking

Traditional EM data are stacked, when the responses of contiguous half-cycles of opposing polarity are subtracted from each other, preserving the signal and eliminating any unsynchronized responses, such as powerline noise. With our objective being the opposite, our processing eliminates the active-source EM response (the primary and secondary EM response induced by the MEGATEM or HELITEM transmitter), in order to improve the S/N ratio of the powerline, VLF and AFMAG signals. This is achieved by stacking the raw responses of each half-cycle in pairs of two without adjusting for the change in polarity. In order for the pulses of two consecutive half-cycles to be identical, the earth-field response (coil-motion noise) is removed before the reverse stacking takes place. The power spectra of x-component MEGATEM data before and after earth-field removal and reverse stacking are shown in Figure 2. Whereas VLF responses can be identified in the y-component power spectrum of Figure 1, the x-component VLF responses cannot be seen in the unprocessed data (Figure 2, left panel), because of the stronger active-source signal, due to the stronger coupling of the x-component receiver coil with the primary field. Figure 2 shows that, due to the nearly perfect symmetry of the MEGATEM half-cycle pulses, the active-source signal gets removed enough by the reverse stacking for the VLF response to become clearly visible. For the HELITEM system, the recorded pulses of consecutive half-cycles show more variation, with reverse stacking not being as effective at reducing the active-source signal. For those data, extracting the VLF response via MSK (minimum shift key) decoding, as suggested by Macnae (2015) and Rasmussen *et al.* (2017) might result in a cleaner VLF signal. Except for one VLF station (VTX2), all stations examined in the case studies discussed below appear to have used MSK modulation.

Spectral Response Extraction

The spectral responses are extracted at selected frequencies as described by Pedersen *et al*. (1994). Powerline responses were extracted at 50, 150 and 250 Hz or 60, 180, 300 Hz, depending on the powerline frequency. AFMAG responses were processed at frequencies in the range 75 - 600 or 90 - 720 Hz. Natural-field and radio-field responses at VLF and LF ranges were extracted from 5 kHz up to the Nyquist frequency of the system's digitisation rate, which ranged from 11.52 to 61 kHz for the discussed data sets. Tests for the South American MEGATEM data included the derivation of narrowband and broadband VLF radio-field responses. The former included 6 separate responses derived from 400 Hz wide frequency bands, centred at the station frequencies; the latter made use of the combined responses of the 6 VLF transmitters in the frequency range 16.8-25.4 kHz. Since the broadband responses covered a range of azimuths, the S/N ratio was better than for the narrowband signals.

Figure 2: Spectral density of x-component MEGATEM high-elevation data (no ground response) before (left) and after (right) earth-field removal and reverse stacking.

Attitude Correction

The attitude-correction of VLF data acquired with a sensor attached to the survey aircraft is described by Bastani and Pedersen (1997). For a towed-bird sensor, a similar approach might be used. An attempt was made to derive the attitude of the receiver coil set from the derived earth-field response and the horizontal-component data from one or more VLF stations in order to apply an attitude-correction to the data.

The earth-field (EF) response is a function of the magnetic field vector, the heading and speed of the plane and the rate of change of the receiver attitude. Model results show that the EF response is fairly insensitive to the actual values of the magnetic field vector, which can be approximated by regional IGRF values. Further, because of the relatively slow speed of the plane, responses due to dragging the receiver coils through lateral magnetic field gradients are negligible when compared to the responses induced by the relatively fast rotation of the coil set. Unfortunately, the EF response is insensitive to any sensor rotation occurring in the plane perpendicular to the magnetic field vector. A singular-value decomposition inversion was used for recovering the receiver attitude from the EF response. Analysis of the eigenvectors and eigenvalues indicated that the coil pitch was well resolved, but roll and yaw are not independently resolved. Requiring additional data to resolve the ambiguity between roll and yaw, the directional information of the VLF data was analysed.

It has been suggested that the azimuths between the sources of VLF signals and sensor locations can be derived from the horizontal components of measured electromagnetic fields (Golkowski and Inan, 2008). Therefore, it was tested if the apparent yaw of a receiver coil could be derived from the VLF radio-field responses as derived from the streamed South American MEGATEM x and y-data, since the actual azimuths between receiver locations and VLF stations are known. Unfortunately, derived apparent azimuths showed a strong sensitivity to the local topography. This suggests that the secondary fields of the horizontal components are too big to be negligible, and hence, the assumption that the responses of the horizontal components are dominated by the VLF primary field is incorrect. This was confirmed with synthetic modelling of the survey terrain using *MT3Dfwd* (Holtham and Oldenburg, 2010). Azimuths derived from the synthetic horizontal magnetic field responses indicate values that are wrong by up to +/- 5 degrees, as a result of the topography. An attempt was made to derive the needed primary horizontal VLF responses via removal of the secondary horizontal VLF responses, derived from the vertical (secondary only) VLF response via Hilbert transformation (Macnae, 1984; Nabighian, 1984). However, results were not encouraging and, hence, tipper data were left uncorrected for receiver attitude.

Tipper Derivation

Stacked cross and auto-spectra are computed at the target frequencies, followed by the derivation of the tipper response (Vozoff, 1972):

$$T_{zx} = \frac{\langle H_z H_x^* \rangle \langle H_y H_y^* \rangle - \langle H_z H_y^* \rangle \langle H_y H_x^* \rangle}{\langle H_x H_x^* \rangle \langle H_y H_y^* \rangle - \langle H_x H_y^* \rangle \langle H_y H_x^* \rangle} \quad (1)$$

$$T_{zy} = \frac{\langle H_z H_y^* \rangle \langle H_x H_x^* \rangle - \langle H_z H_x^* \rangle \langle H_x H_y^* \rangle}{\langle H_x H_x^* \rangle \langle H_y H_y^* \rangle - \langle H_x H_y^* \rangle \langle H_y H_x^* \rangle} \quad (2)$$

We used the same sign convention as applied to ZTEM data (Legault, 2012) in order to facilitate the use of our existing ZTEM modelling software.

Conductivity Models

Conductivity information can be derived from tipper data via grid filter operations, such as phase rotations (Lo *et al*., 2009), the derivation of the *peaker* (Pedersen *et al*., 1994) and apparent conductivity transformations (Becken and Pedersen, 2003). The derivation of these grid products doesn't take into account the topography of the survey area, which can result in mapped conductivity highs across mountains and conductivity lows across valleys. More reliable conductivity information can be extracted from 2D and 3D inversions, taking into account the terrain's topography. These algorithms were originally written for the inversion of MT data, but can be applied for the modelling of VLF and AFMAG data (Sattel and Witherly, 2012; Legault *et al*., 2012). The 2D algorithm used for this study is based on the 2D algorithm developed by Constable and Wannamaker (deGroot-Hedlin and Constable, 1990; deLugao and Wannamaker, 1996). The finite-element algorithm models the Tzx data and takes into account the terrain's topography and the ground clearance of the receiver along the flight line. The 2D assumption implies structures, including the topography to have infinite strike length. A 3D inversion jointly inverts the Tzx and Tzy data of multiple flight lines, also taking into account the terrain topography and sensor elevation. The 3D algorithms used are described by Holtham and Oldenburg (2010) and Haber *et al*. (2012).

CASE STUDIES

MEGATEM South America

The MEGATEM data were acquired at a base-frequency of 25 Hz using a digitisation rate of 51.2 kHz. A close-up of the power spectrum in the VLF frequency range is shown in Figure 3. Strong VLF signals were recorded from VTX2 India, NPM Hawaii, NDT Japan, NAA Maine, NLK Washington and NML South Dakota. The distances of these stations to the survey area range from around 7,000 km to over 17,000 km, and the spatial distribution of these stations provides very good azimuthal coverage.
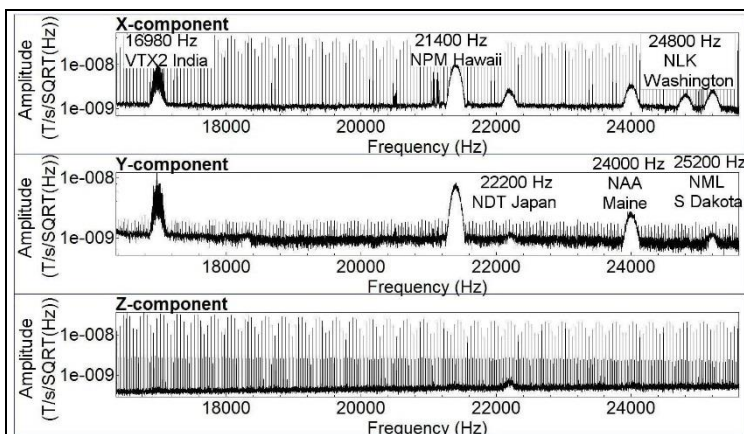

Figure 3: Close-up of Figure 1 showing spectral density of the x-, y- and z-component data in the frequency range 16-24 kHz.
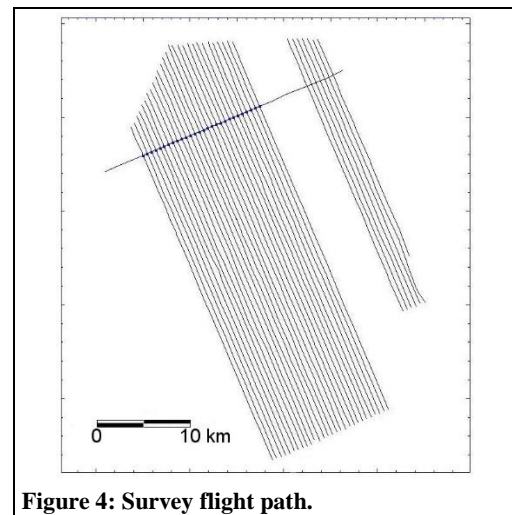

Figure 4: Survey flight path.

The flight path of the examined AEM data, including one tie line, is shown in Figure 4. In order to evaluate the repeatability of the VLF tipper data, Figure 5 shows a comparison of the tie-line profile with the responses extracted along the tie line from the smoothed VLF responses of the other survey lines. The extracted profile has a data point every 400 m (the same as the line spacing) and the extracted data were reassigned Tzx = Tzy and Tzy = -Tzx to be consistent with the tie-line data polarity. The unfiltered tie-line profiles show the effect of sensor motion. Nevertheless, there is fairly good agreement between the two data sets, suggesting good data repeatability.
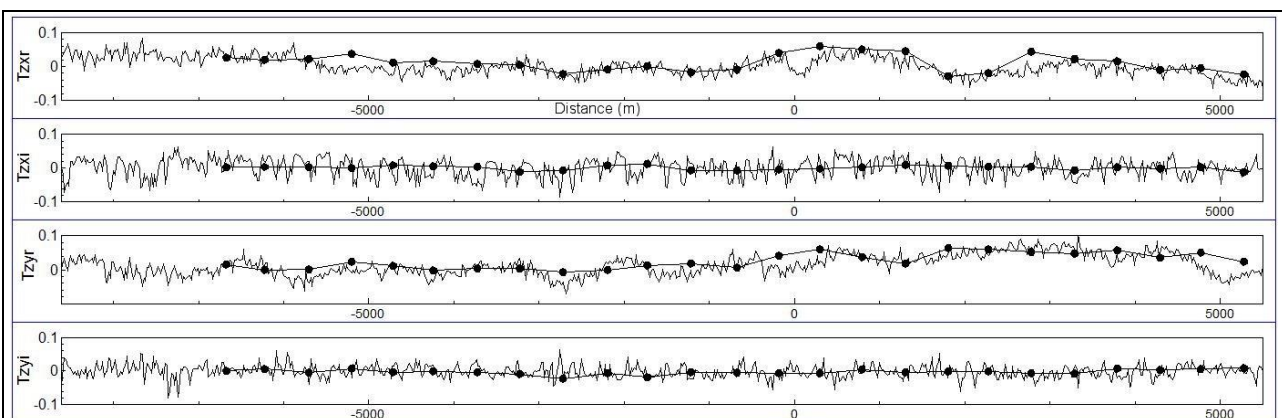

Figure 5: Comparison of the VLF (21,090 Hz) tipper profiles for the tie-line of Figure 4 with tipper data derived from the western block of the NNW-SSE survey lines (dotted lines).

The tipper data for a range of frequencies were transformed to apparent conductivities using the method described by Becken and Pedersen (2003). The results, shown in Figure 6, appear to outline structures related to subsurface conductivities and the terrain's vertical relief, which is severe (1200-4800m). The powerline along the southern border of the survey area appears to provide enough 50 Hz signal to result in a coherent conductivity map. However, results close to the powerline location are probably questionable, due to source effects. The derived AFMAG data have low S/N ratios, which resulted in less coherent apparent conductivity grids. The shown example at 300 Hz appears to indicate structures of elevated conductivities, but in the absence of independent verification their existence is uncertain. In contrast, the VLF natural-field data at 9,600 Hz and the VLF radio-field data at 21,090 Hz have much higher S/N ratios, but are also highly sensitive to topography. That sensitivity facilitates data calibration, but the apparent conductivity grids, which are not compensated for the terrain's topography, are of limited value.
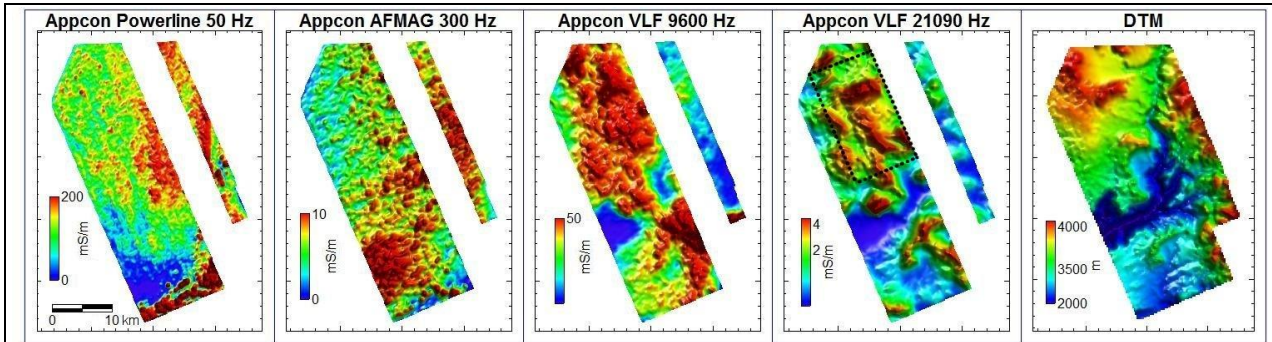

Figure 6: Apparent conductivities derived from powerline, AFMAG and VLF tipper data. A powerline runs along the southern end of the area, as indicated by very high amplitudes on the 50 Hz grid. A strong correlation with the terrain's topography is apparent for the VLF data at 9,600 and 21,090 Hz. The 3D-inverted area, shown in Figure 8, is outlined on the 21,090 Hz grid.

In order to model subsurface structures from the VLF 21,090 Hz tipper data, 2D and 3D inversions were applied. The result of a 2D inversion, using a 1000 Ohm-m half-space as a start model, is shown in Figure 7. From our experience and published results (Legault *et al*., 2012, Spies, 1989), 1.5 times the skin depth is a good estimate of the depth penetration for MT and AFMAG data. The estimated depth range of the VLF data, derived from 1.5 times the skin depth at 21,090 Hz, is indicated by the dashed line on the conductivity-depth section. The strong VLF crossover response across the valley should be noted. The inversion result indicates that the top of the conductive layer can be mapped from the VLF data. Also shown is the conductivity-depth section (CDS) derived via layered-earth inversions from the active-source MEGATEM data. The latter has a deeper depth range than the VLF-derived CDS, but the derived conductivities agree well at shallow depths. 3D inversion results of a survey subset of the 21,090 Hz Tzx and Tzy data are shown in Figure 8. The shallow conductivity slices compare well with the square-wave processed channel 1 amplitudes (Sattel and Battig, 2016), confirming that valuable information can be derived from the VLF data.
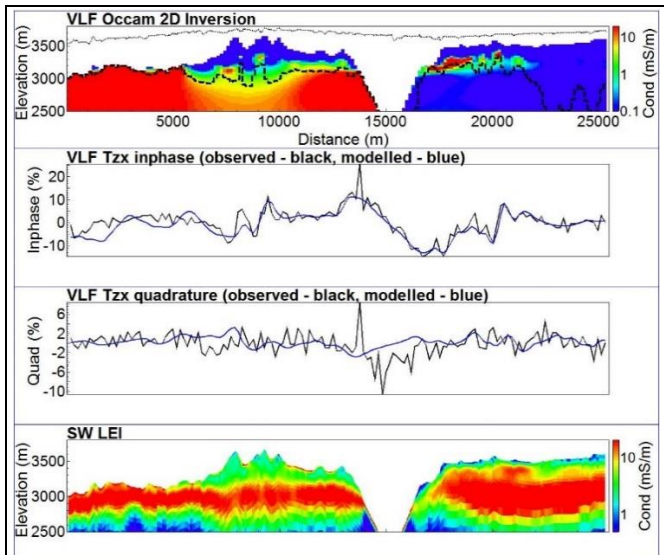

Figure 7: Conductivity-depth section derived by 2D inversion from VLF tipper data (top), corresponding observed and modelled tipper profiles and 1D inversion result from square-wave processed active-source EM data (bottom). In the top panel, the EM bird elevation is shown with a dotted line, the approximate penetration depth, which represents 1.5 skin depths is indicated by a dashed line.
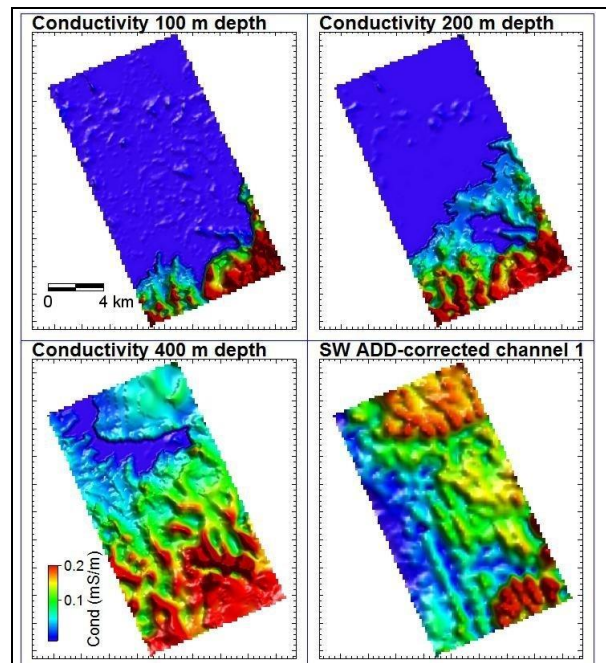
Figure 8: Conductivity-depth slices derived by 3D inversion from VLF tipper data and square-wave ADD-corrected channel 1 amplitudes.

MEGATEM Timmins, Ontario, Canada

MEGATEM data acquired near Timmins, Ontario, Canada by the Geological Survey of Canada (GSC) in 2002 using a base-frequency of 30 Hz and a digitisation rate of 23,040 Hz were analysed for AFMAG and powerline EM responses. The sampling frequency is too low for extracting EM responses in the range of VLF radio fields. The survey flightpath is show in Figure 9 along with the channel 10 z-component response of the active-source EM data, as provided by CGG and the derived apparent conductivity grids derived from the tipper data extracted for 30 Hz (AFMAG) and 60 Hz (powerline). A major powerline crosses the area, the location clearly visible on the channel 10 amplitude grid just east of the survey centre. The 30 Hz apparent-conductivity grid doesn't appear to indicate any conductivity structure, besides the location of the powerline. In contrast, the 60 Hz apparent-conductivity grid appears to outline broader structures that are less apparent from the EM channel 10 amplitude grid.
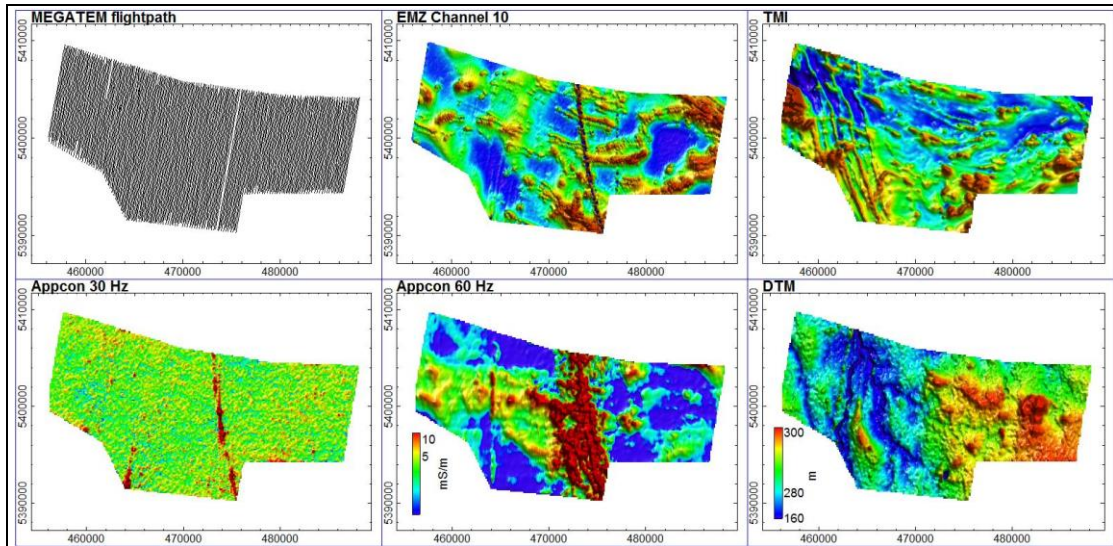

Figure 9: Survey flightpath and grids of EM channel 10 amplitude, TMI, apparent-conductivity grids at 30 and 60 Hz and the topography.

HELITEM Kluane Lake West, Yukon, Canada

The HELITEM data were acquired at a base-frequency of 30 Hz and a digitisation rate of 122 kHz. The power spectrum in the VLF frequency range is shown in Figure 10. Strong VLF signals were recorded from stations as far away as NWC Australia. The locations of the VLF stations in relation to the survey area are shown in Figure 11. The spatial distribution indicates excellent azimuthal coverage.
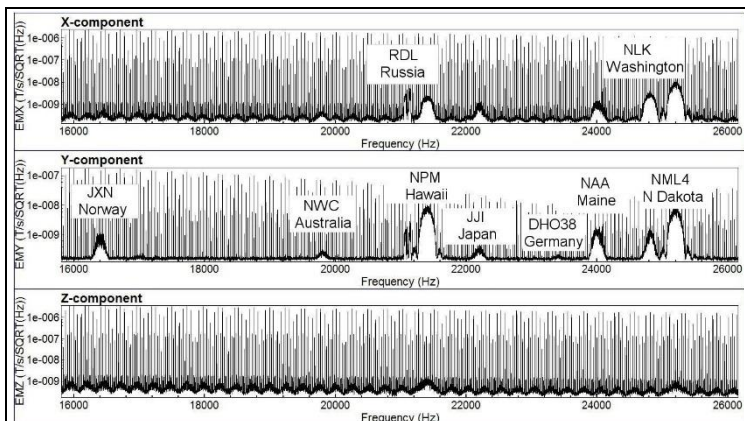
Figure 10: Spectral density of the x-, y- and z-component data in the frequency range 16-26 kHz.
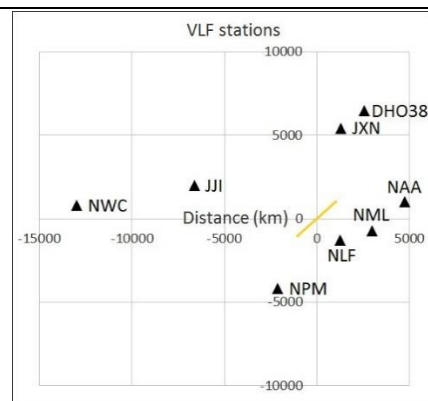

Figure 11: VLF station locations in relation to survey area, indicated by yellow line (survey line not drawn to scale).

Apparent conductivity grids derived at various frequencies are shown in Figure 12, along with other survey results, including early- and late-time τ (decay constant) grids derived from the active-source EM data. The latter indicate conductivity structures striking NW-SE, perpendicular to the flight lines. Tipper responses at 20.9 and 43.6 kHz were forward modelled with program *MT3Dfwd* using the digital terrain model (DTM) and assuming a 1000 Ohm-m half-space, followed by the derivation of apparent conductivities. The observed apparent conductivity grid at 20.9 kHz (16.2 – 25.6 kHz range) agrees well with the predicted values, but shows more spatial detail, suggesting that the VLF responses are dominated by the terrain's topography, but also contain information about the subsurface conductivity structure. Even though the LF response at 43.6 kHz relies on natural fields, a weak correlation between the predicted and

observed apparent conductivities is apparent. Without any major powerline in the vicinity of the survey area and weak natural fields, the 60 Hz apparent conductivity grid appears to be dominated by noise. Apparent conductivities at 720 Hz and 9.6 kHz appear to show some spatial patterns that might correspond to deeper conductivity structures.
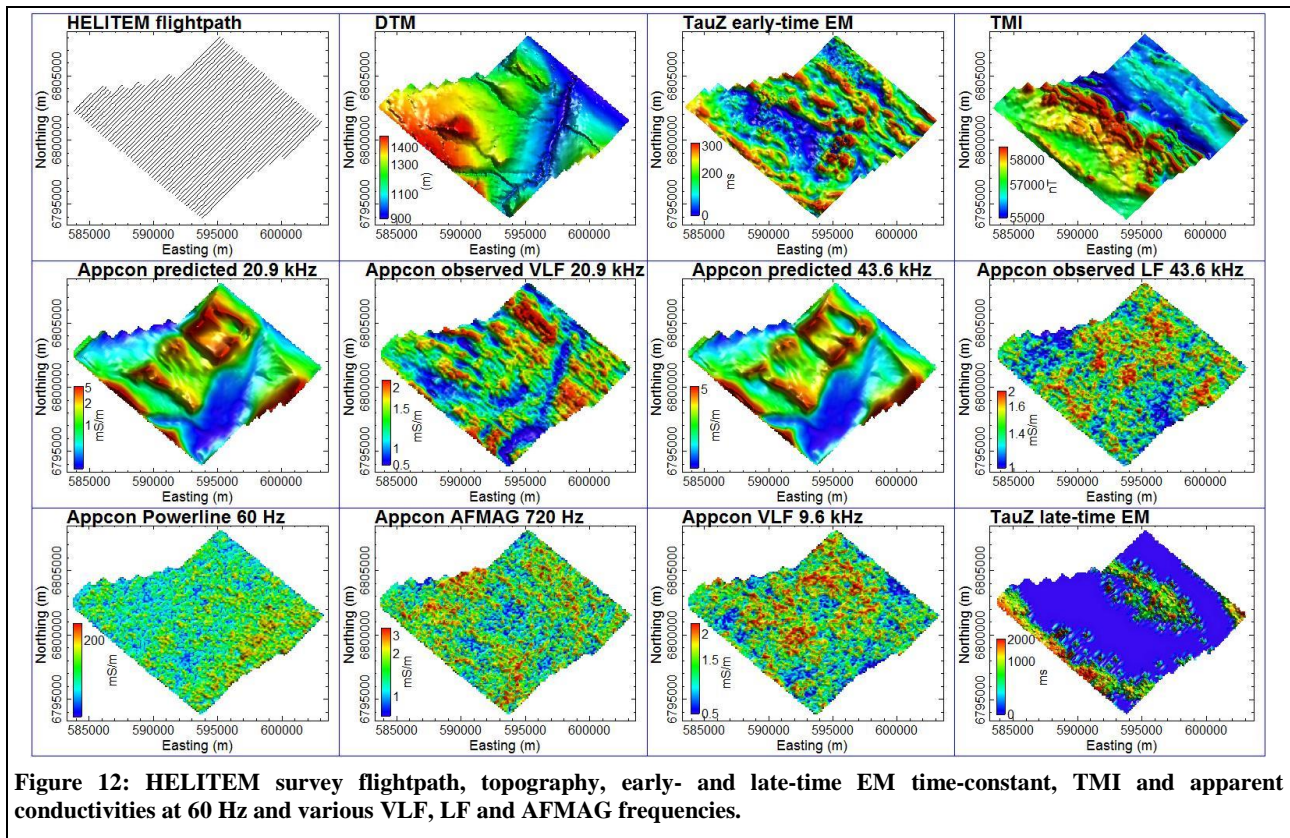
Figure 12: HELITEM survey flightpath, topography, early- and late-time EM time-constant, TMI and apparent conductivities at 60 Hz and various VLF, LF and AFMAG frequencies.

CONCLUSIONS

The discussed field data results show that the extraction and modelling of powerline and VLF tipper data can provide complementary conductivity information of the survey area. VLF responses are strongly related to the survey topography and, in rugged survey terrain, 2D and 3D inversions have to be used to map subsurface conductivity structures. The quality of extracted AFMAG data is poor, but could be substantially improved by monitoring and correcting for receiver attitude.

ACKNOWLEDGMENTS

REFERENCES

Bastani, M., and L.B. Pedersen, 1997, The reliability of aeroplane attitude determination using the main geomagnetic field with application to tensor VLF data analysis: Geophysical Prospecting, 45, 831-841.

Becken, M., and L.B. Pedersen, 2003, Transformation of VLF anomaly maps into apparent resistivity and phase: Geophysics, 68, 497-505.

Bosch, F.P., and I. Műller, 2005, Improved karst exploration by VLF-EM-gradient survey: comparison with other geophysical methods: Near Surface Geophysics, 3, 299-310.

DeGroot-Hedlin, C., and S. Constable, 1990, Occam's inversion to generate smooth two-dimensional models from magnetotelluric data: Geophysics, 55, 1613-1624.

DeLugao, P.P., and P. Wannamaker, 1996, Calculating the two-dimensional magnetotelluric Jacobian in finite elements using reciprocity: Geophysical Journal International, 127, 806-810.

Golkowski, M., and U.S. Inan, 2008, Multistation observations of ELF/VLF whistler mode chorus: Journal of Geophysical Research, 113, A08210.

Haber, E., E. Holtham, J. Granek, D. Marchant, D. Oldenburg, C. Schwarzbach, and R. Shekhtman, 2012, An adaptive mesh method for electromagnetic inverse problems: SEG conference, expanded abstracts.

Holtham, E., and D.W. Oldenburg, 2010, Three-dimensional inversion of ZTEM data: Geophysical Journal International, 182, 168-182.

Kamm, J., and L.B. Pedersen, 2014, Inversion of airborne tensor VLF data using integral equations: Geophysical Journal International, 198, 775-794.

Labson, V.F., and H.G. Medberry, 1989, Airborne resistivity mapping using powerline sources: 59th Annual Meeting, SEG, Expanded Abstracts, 138-140.

Labson, V.F., A. Becker, H.F. Morrison and U. Conti, 1985, Geophysical exploration with audiofrequency natural magnetic fields: Geophysics, 50, 656-664.

Legault, J.M., 2012, Ten years of passive airborne AFMAG EM development for mineral exploration: 82nd International Exposition and Annual Meeting, SEG, Expanded Abstracts.

Legault, J.M., S. Lombardo, S. Zhao, J. Clavero, I. Aguirre, R. Arcos and E. Lira, 2012, ZTEM airborne AFMAG EM and ground geophysical survey comparisons over the Pampa Lirima geothermal field in northern Chile: Geotech website.

Lane, R., C. Plunkett, A. Price, A. Green and Y. Hu, 1998, Streamed data - a source of insight and improvement for time domain airborne EM: Exploration Geophysics, 29, 16-23.

Lo, B., J. Legault, P. Kuzmin and M. Combrinck, 2009, Z-TEM (airborne AFMAG) tests over unconformity uranium deposits: ASEG conference, extended abstracts.

Macnae, J., 2015, Stripping very low frequency communication signals with minimum shift keying encoding from streamed time-domain electromagnetic data: Geophysics, 80, E343-E353.

Macnae, J., 1984, Survey design for multicomponent electromagnetic systems: Geophysics 49, 265-273.

Nabighian, M.N., 1984, Toward a three-dimensional automatic interpretation of potential field data via generalized Hilbert transforms: Fundamental relations: Geophysics 49, 780-786.

Nyboe, N.S and S.S. Mai, 2017, Recent advances in Skytem receiver system technologies: EAGE Near Surface Geoscience conference, Extended Abstracts.

Pedersen, L.B., W. Qian W., L. Dynesius and P. Zhang, 1994, An airborne tensor VLF system. From concept to realization: Geophysical Prospecting, 42, 863-883.

Rasmussen S., N.S. Nyboe, S.S. Mai and J.J. Larsen, 2017, A robust framework for cancellation of MSK interference in TEM data: EAGE Near Surface Geoscience conference, Extended Abstracts.

Sattel, D., and E. Battig, 2018, Square-wave processing of MEGATEM data: AEGC conference, Extended Abstracts.

Sattel, D., and E. Battig, 2016, Reprocessing streaming MEGATEM data for square-wave EM, VLF and AFMAG responses: 86th Annual Meeting, SEG, Expanded Abstracts, 2144-2148.

Sattel, D., and K. Witherly, 2012, An overview of ZTEM interpretation tools, In R.J.L. Lane (editor), Natural Fields EM Forum 2012: Abstracts from the ASEG Natural Fields EM Forum 2012: Published by Geoscience Australia, Geoscience Australia Record 2012/04.

Spies, B., 1989, Depth of investigation in electromagnetic sounding methods: Geophysics 46, 1137-1147.

Vallee M.A., R.S. Smith and P. Keating, 2010, Case history of combined airborne time-domain electromagnetics and power-line field survey in Chibougamau, Canada: Geophysics, 75, B67-B72.

Vozoff K., 1972, The magnetotelluric method in the exploration of sedimentary basins: Geophysics, 37, 98-141.

Ward, S.H., J.O. O'Donnell, R. Rivera, G.H. Ware and D.C. Fraser, 1966, AFMAG – applications and limitations: Geophysics 31, 576-605.